Water-Oil Displacement in Shale: New Insights from a Comparative Study Integrating Imbibition Tests and Multiscale Imaging

Sheng Peng[1, *], Pavel Shevchenko[2], Priyanka Periwal[1], Robert M. Reed[1]

1. Bureau of Economic Geology, Jackson School of Geosciences, The University of Texas at Austin, University Station, Box X, Austin, Texas 78713, USA

2. Advanced Photon Source, Argonne National Laboratory, Lemont, IL 60439, USA

[*]Corresponding author email: sheng.peng@beg.utexas.edu

Summary: Water-oil displacement is an important process that occurs in a shale matrix after hydraulic fracturing and in water-based enhanced oil recovery. Current understanding of this displacement process is limited because of the complicated pore structure and surface properties in shale. In this work, this process and its controlling factors are investigated through a comparative study of three shale samples that have different types of pore systems and wettability. An integrated method of imbibition and multiscale imaging was applied, and a modified oleic tracer that can better represent oil flow was used in imbibition testing and micro-CT imaging. SEM pore characterization was then performed under high magnification with guidance from the micro-CT images showing the changes due to oil or water imbibition. New insights were obtained on the importance of both wettability and pore size effect on oil recovery and the distribution of residual oil after water-oil displacement. Connectivity of pores with different wettability is also discussed on the basis of 3D analysis and SEM pore characterization. Collectively, these new findings improve the understanding of the complicated process of water-oil displacement and the role of influencing factors. Important implications for improved oil recovery strategy in shale are discussed for different types of reservoir rocks. The integrated imaging and imbibition technique provides a new path for further investigation of improved oil recovery in shale.

Keywords: water-oil displacement, shale, wettability, pore type, pore structure, connectivity

Introduction

Water-oil displacement is an important process that occurs in hydraulic fracturing and enhanced oil recovery with water-based agents in shale oil reservoirs. It is also relevant to water-oil distribution during oil generation and expulsion and after hydraulic fracturing, and consequently affects water-oil two-phase flow during production. Because of the complicated surface properties of the pore systems, unclear connectivity of pore networks with different wetting properties, and the small pores and low porosity, an understanding of water-oil displacement in shale and its controlling factors are still limited.

Wettability is a key influencing factor in water-oil displacement and distribution, and many previous works have focused on wettability characterization in shale (e.g., Roshan et al. 2016; Gupta et al. 2018; Gao et al. 2019; Lu et al. 2019; Pan et al., 2020a; Arif et al. 2021). Unlike conventional reservoir rocks, which have a relatively simple mineralogical composition and thus relatively more uniform wettability, wettability of shale is more complex owing to a wider variation of mineralogy and organic-matter content. In general, quartz and major types of clay minerals, i.e., illite and smectite, are more water-wet, whereas kaolinite is potentially oil-wet (Borysenko et al. 2009; Pan et al. 2020b). Organic matter and calcite are more oil-wet, but calcite can be water-wet as well at a certain pH and salinity (Chen et al. 2018). The type and maturity of organic matter can also affect wettability (Begum et al. 2019; Jagadisan and Heidari 2019). However, determination of wettability of a shale sample on the basis of bulk mineralogy and total organic carbon (TOC) can be misleading sometimes because it is the local mineralogy and organic-matter distribution surrounding the pores that control the pore wettability. This local mineralogy is normally different from bulk mineralogy and TOC (Peng et al. 2019). For example, the dominant minerals in a carbonate floatstone (sample W1 in Peng et al. (2019a)) are calcite and quartz, accounting for ~80% weight fraction based on XRD analysis; however, the dominant pore type in that sample is clay mineral pores. Contact angle measurement on the sample surface thus is more reflective of the wetting property of the dominant minerals, that is, calcite and quartz, and is less relevant to the pore wettability which instead is controlled by clay mineral (Peng et al., 2019a). Therefore, pore wettability needs to be evaluated based on the pore surface mineralogy and organic-matter distribution.

Several methods have been applied for shale wettability quantification or characterization, including contact angle measurement, spontaneous imbibition, and the Nuclear Magnetic Resonance (NMR) wettability index (NWI) method. Contact angle measurement using the sessile drop method often generates results contradictory to other tests, such as spontaneous imbibition in shale (Engelder et al. 2014; Singh 2016; Peng and Xiao 2017; Siddiqui et al. 2018). Nevertheless, contact angle measurement may reflect the wetting property of fractures because fractures develop across the main body of the rock, thus the surface of fractures has similar mineralogy to the bulk mineralogy (Peng et al 2019a).

Spontaneous imbibition has become a popular technique for shale research in recent years (e.g., Gao and Hu 2016; Roshan et al. 2016; Alvarez and Schecter 2017; Gao et al. 2019). Spontaneous imbibition is also often combined with NMR saturation determination (Ali et al. 2020). Studies using this method provided important insights including imbibition rates, relative wettability of oil or water to gas, and pore size distribution of the wetting and non-wetting phases.

An NWI method initially developed for carbonates (Looyestijn and Hofman 2006) has been applied for the quantification of shale wettability recently (Dick et al., 2019; Kelly et al., 2020). The NMR wettability index is derived based on T_2 measurement and a pore-size-dependent relaxation model in which both the effects of wetting-phase surface and nonwetting-phase saturation on NMR response are considered simultaneously (Looyestijn and Hofman 2006). This NMR wettability index can thus represent the wettability more accurately in a scenario where the wetting phase covers the surface of a pore but does not displace the nonwetting phase in the pore completely.

Nevertheless, all the techniques mentioned above are a “black-box” type of method, and thus are unable to resolve the spatial distribution of the wetting and nonwetting pore system and potential heterogeneity, which can be important in elucidating the underlying geological controls on wettability in shale.

Albeit wettability is critical in water-oil displacement, other factors, including pore size and connectivity, also play important roles. Peng et al. (2019a) show that pore aspect ratio (body and throat size ratio) can affect water-oil displacement and oil recovery. Specifically, oil recovery by water imbibition is less efficient in pores with a larger pore aspect ratio when pore throat size is similar (Peng et al. 2019a). However, attention has not been paid adequately to the pore size effect on water-oil displacement in shale. Connectivity of pores with different wetting properties is poorly understood, although many works assume an independent dual-wet system in shale (e.g., Yassin et al. 2016). Further study and elucidation of the effect of pore size and connectivity on water-oil displacement is needed.

In this paper, a systematic investigation of water-oil displacement is conducted through an integrated water-oil spontaneous imbibition and multiscale imaging technique for samples with different wettability. Analysis of oil and water imbibition in mm-scale samples is combined with nano-to-micro-scale pore system characterization. This way, more specific and comprehensive understanding of the mechanisms and influencing factors, including wettability, pore size, and connectivity, of water-oil displacement in shale is achieved. Implications of the results for improved oil recovery in shale oil reservoirs are also discussed.

Materials and Methods

Samples. Three samples, one from the Wolfcamp Shale (S1) and two from the Eagle Ford Shale (S2 and S3), were used in this study (**Table 1**). These samples were selected based on a preliminary screening test in which different levels of water-oil displacement were observed. The samples contain different lithofacies, with S1 to S3 being argillaceous siliceous siltstone, calcareous siliceous mudstone, and organic-rich calcareous mudstone, respectively. They have similar thermal maturities with Ro values of 0.8–1.0% (Ko et al. 2017). The influence of maturity on wettability and water-oil displacement is not within the scope of this work.

A mini-plug with a diameter of 1.5 mm was obtained from a 1-inch-diameter plug for each sample. The same mini-plugs were used for oil and water spontaneous imbibition and multiscale imaging. Measurement of porosity and permeability was conducted on a sister 1-inch plug that was obtained at an adjacent location for each sample using the modified gas-expansion (MGE) method (Peng et al. 2019b). The MGE method is a transient method that calculates the matrix permeability on the basis of the measured pressure decay curve. The measurement was performed under a pore pressure of ~150 psia and a net stress of 2000 psi. All plug samples were drilled parallel to the bedding direction and were dried at 110˚C for 3 d in a vacuum oven to remove residual moisture before the experiments.

Table 1. Geological and petrophysical information for the samples used in this study.

Sample #	Formation	Depth (ft)	Porosity	Permeability (nD)	TOC	Rock description and bulk mineralogy (from Ko et al. 2019)
1	Wolfcamp	7,732	6.4%	560	1.68%	Argillaceous siliceous siltstone with 19% calcite, 51% quartz, and 25% clay
2	Eagle Ford	11,901	3.5%	400	2.56%	Calcareous siliceous mudstone with 31.4% calcite, 34.6% quartz, and 15% clay
3		12,308	7.4%	478	3.29%	Organic-matter-rich calcareous mudstone with 65.5% calcite, 18% quartz, and 8% clay

A modified oleic tracer. Micro-CT imaging of fluid distribution in shale is challenging because of the nanoscale pores and the limited resolution in micro-CT. An oleic X-ray contrast agent, diiodomethane (DIM, 99%), made the micro-CT imaging of the fluids in shale possible (Fogden et al. 2014a; Fogden et al. 2014b) and was used as an oil-phase tracer in a study of multiphase flow in shale (Peng and Xiao 2017; Peng et al. 2019a). However, DIM shows a big difference in wetting property from the real oil. The contact angle of DIM on a glass plate (39.8° in air and 118° in water) is substantially larger than a paraffin-type hydraulic oil (13.5° in air and 72.5° in water) (**Fig. 1**). Dodecylbenzene (C12B, VWR, 97%) was added to DIM as a surface-tension modifier. The benzene group in C12B acts as a surfactant head group with high affinity for DIM and the alkyl chain as a surfactant tail group with low affinity for the DIM solvent (Fletcher and Nicholls 2000). Approximately 1.5 mol% C12B was added and mixed with DIM overnight to form a stable miscible mixture. The additive lowered the surface tension of DIM from 51 to 34 mN/m (Fletcher and Nicholls 2000), and the C12B+DIM mixture shows similar contact angles (16° in air and 78.5° in water) with the paraffin oil (**Fig. 1**), indicating a similar wetting property, and thus can represent oil flow better. The small fraction of C12B showed minimal impact on the contrast enhancement effect of DIM in micro-CT imaging through a preliminary test.

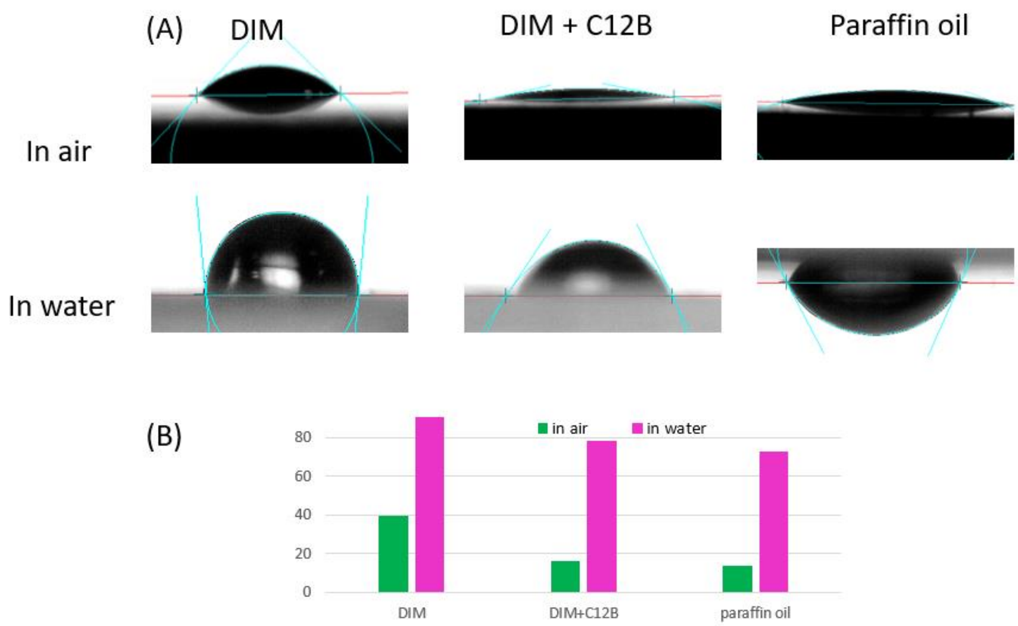

Fig. 1—Contact angle measurement of DIM, DIM+C12B, and the paraffin oil on a glass plate. (A) Snapshots of the sessile drop tests; (B) comparison of the contact angle.

Contact angle was measured using the sessile drop method with an OCA 15EC (DataPhysics Instruments). A glass plate was used for the contact angle measurement to signify the change of wetting property of the fluids. A small volume of fluid (~0.5 µL) was applied to the glass plate surface and covered an area with a diameter of about 0.5–1 mm. Four to six measurements were conducted at different locations, and the averages were used for each test. The glass plate was cleaned using acetone and water after each measurement.

Spontaneous imbibition and micro-CT imaging. Micro-CT imaging was conducted for the samples under the dry condition first. Scanning was focused on a 1.2-mm section that is 1.2 mm above the bottom surface of the mini-plugs. The pixel resolution is 0.65 µm. The ends of the samples (~1 mm) were then dipped into the DIM+C12B mixture ("oil" hereafter for simplicity) for 24 h to initiate oil imbibition. Ex-situ micro-CT imaging was performed after oil imbibition. The oil-imbibed samples were then submerged in water completely for approximately 17 h to allow water spontaneous imbibition. These time durations are considered adequate for complete oil and water imbibition according to the results of the preliminary study, in which imaging was conducted at every hour and the grayscale after 3-4 h of oil imbibition and 4-8 h of water imbibition is basically stable. The samples were kept submerged in water during micro-CT scanning after water imbibition to ensure that loss of oil, if any, was caused by water-oil displacement rather than evaporation from the surface. The experiments were carried out using the synchrotron-based micro-CT imaging facility at beamline 2-BM of the Advanced Photon Source at Argonne National Laboratory. More detailed information on micro-CT scanning parameters is included in Peng and Xiao (2017).

Micro-CT image processing was performed for image registration and to identify the areas with residual oil (residual oil areas) and where oil was displaced by water (water-imbibed areas) using Avizo (Thermal Fisher FEI) and ImageJ (Schneider et al. 2012). Connectivity of the residual oil and water-imbibed areas was evaluated based on 3D image analysis. Micro-CT-image guided SEM image analysis was then performed for nano- to microscale pore system characterization. The readers are referred to Peng et al. (2019a) for more detailed methods and procedures of imaging processing.

SEM/EDS pore characterization. After micro-CT imaging, the same mini-plugs were dried, ion milled, and used for SEM examination under higher magnification. Because SEM and micro-CT images were obtained for the same sample, a reliable comparison of these images can be made based on the relative positions, shapes, and grayscale of each type of mineral grain. SEM imaging was conducted on a field-emission FEI Nova NanoSEM 430 equipped with two 30-mm^2 Bruker XFlash silicon-drift X-ray energy dispersive spectroscopy (EDS) detectors for elemental identification. Backscattered electron (BSE) and secondary electron through-lens detector (TLD) images were collected at a working distance of ~6 mm and an accelerating voltage of 15 keV. Mineral components were identified using elemental mapping by SEM-EDS detectors operated at an accelerating voltage of 15 keV and a working distance of 10 mm.

Results and Discussion

Sample 1 – an argillaceous siliceous siltstone

Micro-CT image analysis. Remarkable changes are observed among the registered micro-CT images at the dry, after oil-imbibition, and after water-imbibition conditions (**Fig. 2** and **Fig. A-1**), indicating the imbibition of oil into the dry sample and then the water-oil displacement in the oil-saturated sample. **Fig. 2** focuses on the yellow-boxed area in **Fig. A-1** (in Appendix) and shows the change better.

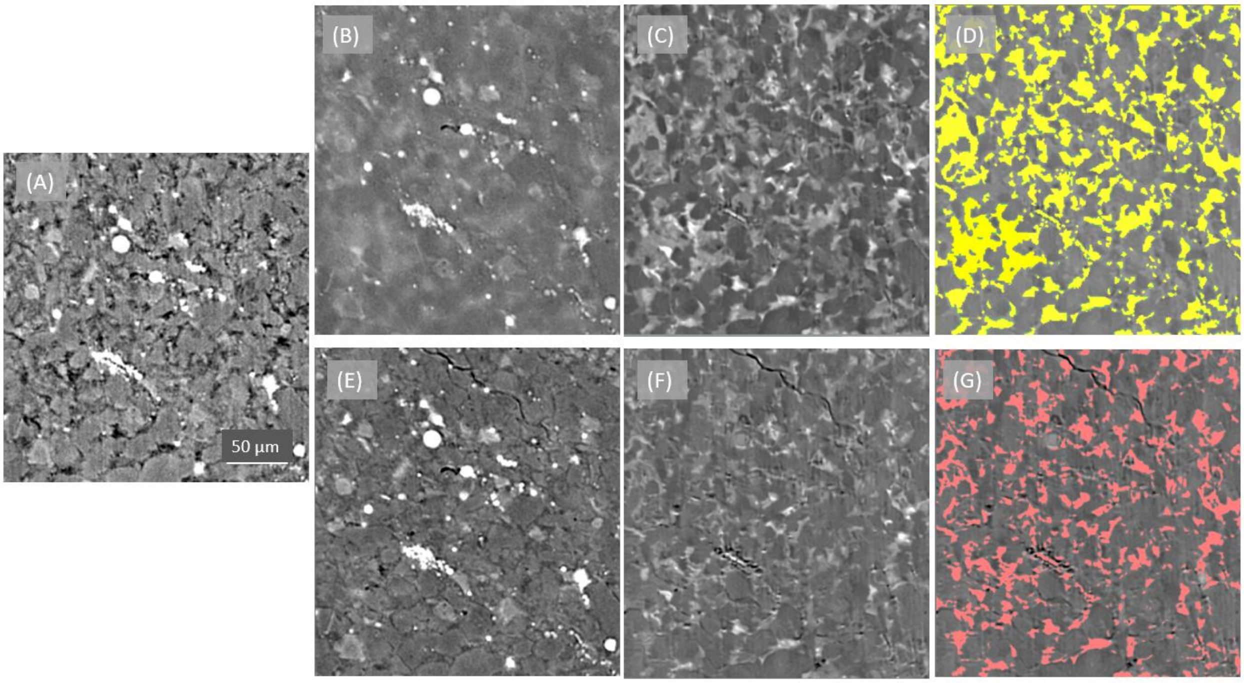

Fig. 2—Micro-CT images of S1 at different conditions and the image calculation/processing results. (A) Dry scan; (B) after oil imbibition; (C) result image of (B – A), lighter areas are where oil imbibition occurs; (D) segmentation result of C, yellow represents oil-imbibed areas; (E) after water imbibition; (F) result image of (E – A), lighter areas contain residual oil after water-oil displacement; (G) segmentation result of F, red represents residual oil areas.

DIM causes stronger X-ray attenuation and results in lighter grayscale in the image. Note that the strong DIM attenuation makes not only the pores brighter but also nearby areas brighter because of the partial volume effect (Ketcham & Carlson 2001). Therefore, the lighter areas are not all pores but are porous. Oil imbibition occurs in most areas between the 10–50 µm scale grains in S1, as indicated by the comparison of the dry image (**Fig. 2A**) and the oil-imbibed image (**Fig. 2B**). **Fig. 2C** is the image calculation result of (**Fig. 2B** (yellow) – **Fig. 2A** (red)) and thus highlights the change due to oil imbibition. In **Fig. 2C**, the lighter areas are the porous areas where oil imbibition occurs; the darker areas are the grains that experience no oil imbibition because they are nonporous or only have isolated intraparticle pores. **Fig. 2D** highlights the oil-imbibed areas in yellow.

Water imbibition only occurs in part of the oil-imbibed areas. The result of (**Fig. 2E** – **Fig. 2A**), that is, subtracting the dry image (**Fig. 2A**) from the water-imbibed image (**Fig. 2E**), highlights the change due to residual oil after water-oil displacement (**Fig. 2F**), which is denoted by the lighter areas in **Fig. 2F**. Comparing **Figs. 2G** and **2D** reveals that a substantial fraction of the porous areas still has residual oil, which in turn means water-oil displacement occurred in the other fraction of the porous areas in S1. Subtracting the residual oil areas from the total oil imbibition areas, that is (**Fig. 2D** (yellow) – **Fig. 2G** (red)), gives the water-imbibed areas (the green areas in **Fig. 3B**). **Fig. 3C** shows the residual oil areas (red) with the dry image background. The combination of the water-imbibed and residual oil areas with the dry image background (**Fig. 3A**) shows that these two areas are adjacent to each other.

Distinct grayscale of the porous areas (in the dry image) is seen between the water-imbibed and residual oil areas in S1. The porous areas in the sample with water imbibition or residual oil are obtained through image processing using "mask" in Avizo (**Figs. 3E** and **3F**). The green (**Fig. 3B**) or red (**Fig. 3C**) areas were used as masks to extract the underlying areas from the dry image to facilitate the study of the underlying mineralogy. **Fig. 3E** is the porous areas (in the dry image) where water imbibition occurred, and **Fig. 3F** is the porous areas having residual oil. Compared to the porous areas with residual oil, where the grayscale is mostly either dark or very bright (**Fig. 3F**), the areas of water imbibition have intermediate grayscale (**Fig. 3E**). This distinct difference provides a guide for the subsequent SEM analysis based on the dry sample, as will be discussed later.

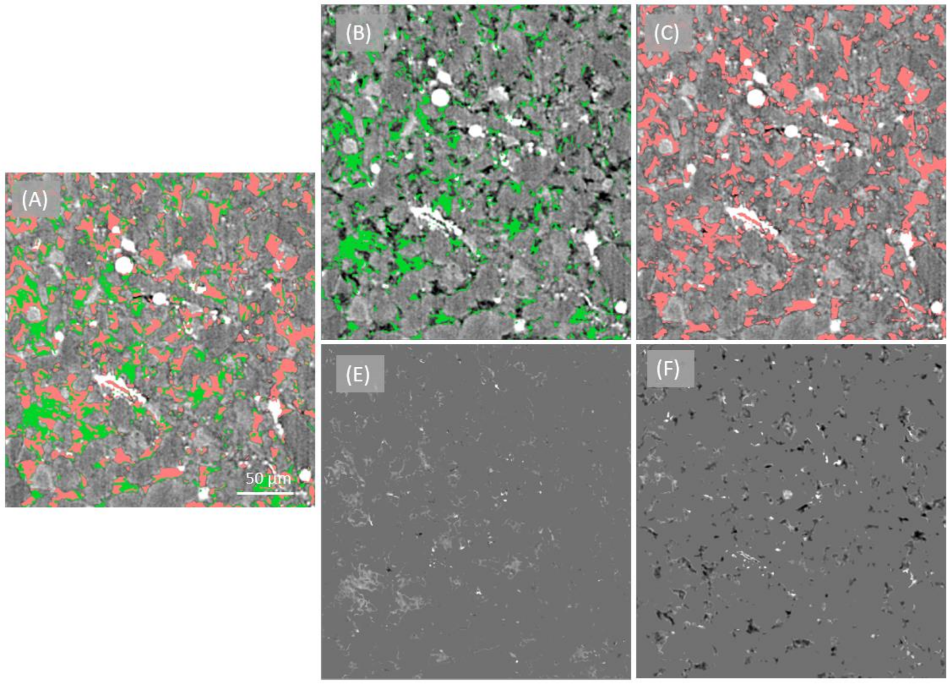

Fig. 3—Image calculation/processing results of the images shown for S1 in Fig. 2. (A) The combination of water-imbibed areas (green) and residual oil areas (red) with the dry image in background; (B) water-imbibed areas (green); (C) residual oil areas (red); (E) extracted areas of green in (B) from the dry image, showing the areas with water imbibition in the dry sample; (F) extracted areas of red in (C) from the dry image, showing the areas with residual oil in the dry sample.

Note that the water-imbibed (green) and residual oil (red) areas do not exclusively contain only water or oil, respectively. **Fig. 2F** divided by **Fig. 2C** produces the residual oil factor (**Fig. 4B**). Comparison of **Figs. 4A** and **4B** reveals that water-imbibed areas have a smaller residual oil factor, meaning small amounts of oil still remained, whereas residual oil areas have a larger residual oil factor, indicating small fractions of water imbibition also occurred (examples in the circled areas in **Figs. 4A** and **4B**). The overall residual oil factor is approximately 50%, meaning 50% of oil has been recovered by water imbibition.

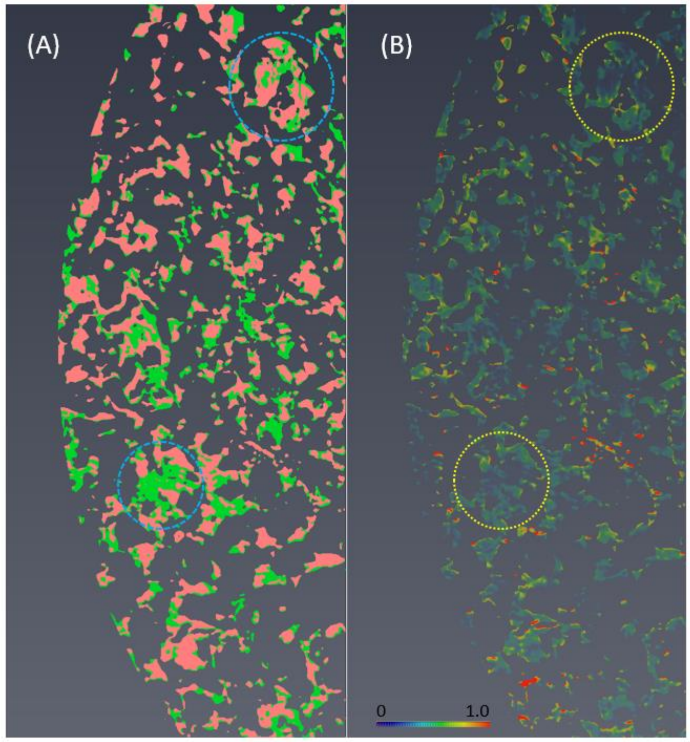

Fig. 4—Residual oil factor map (B) in water-imbibed and residual oil areas (A). Red and green in (A) denote the residual oil and water-imbibed areas, respectively. Scale bar in (B) is the residual oil factor after water imbibition from 0 to 1.0.

3D analysis shows the connectivity of the water-imbibed and residual oil areas (**Fig. 5**). It can be seen that the residual oil areas (**Fig. 5A**) and the water-imbibed areas (**Fig. 5B**) have formed independently connected networks. These two entangled pore networks must be interconnected at the same time (**Fig. 5C**) because the red and green areas are generally adjacent to each other (**Fig. 4A**). Together they combined to the yellow areas in **Fig. 2D** that consist of the total porous areas of this sample. The percentage of water-imbibed and residual oil areas through the 3D analysis are 43% and 57%, respectively.

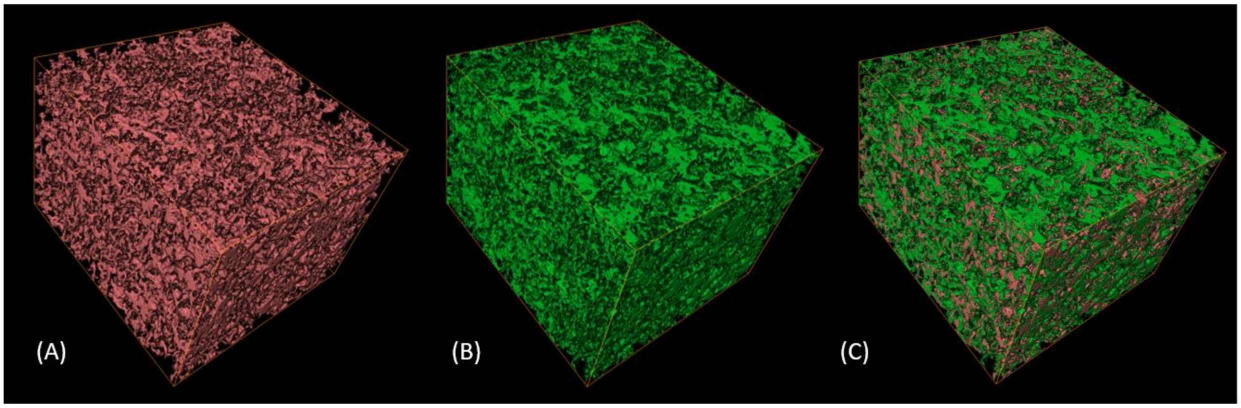

Fig. 5—3D images showing the independently connected networks of the residual oil areas (A) and the water-imbibed areas (B). These two networks are interconnected at the same time in the 3D space (C).

The independent yet interconnected networks demonstrate the complexity of the water and oil flow path and distribution in the sample. The water-imbibed areas are more water-wet, obviously, because water displaced oil; however, whether the residual oil areas are more oil-wet needs further confirmation because oil can also exist in water-wet pores by capillary entrapment. To fully understand the result of water-oil displacement and distribution and the wettability in S1, more detailed investigation of the pore systems in the different colored areas is needed.

SEM pore characterization. BSE grayscale intensity is based on the *Z* value of the minerals, which relates to the atomic numbers of the constituent elements; therefore, BSE images have a similar appearance to micro-CT images. The distinct grayscale in the water-imbibed and residual oil areas from the micro-CT images (**Figs. 3E** and **3F**) can thus guide the SEM pore characterization.

The residual oil areas are either dark or bright, whereas the water-imbibed areas have intermediate grayscale. The areas that have different grayscale are identified from the BSE image of the same sample, and **Fig. 6** shows an example. In **Fig. 6A**, the red-circled areas are the dark areas, or residual oil areas, whereas the green-circled ones are the intermediate grayscale areas, i.e., water-imbibed areas. SEM images at higher magnifications show that interparticle pores are the major pore type between clay mineral grains (“clay mineral pores”) in both areas (**Figs. 6B**, **6D**, **6F**, **6H**). This observation is confirmed by the EDS map of the sample, which shows that clay is the dominant mineral in the porous areas of the entire sample (**Fig. A-2A**). Illite is the main clay mineral type in S1.

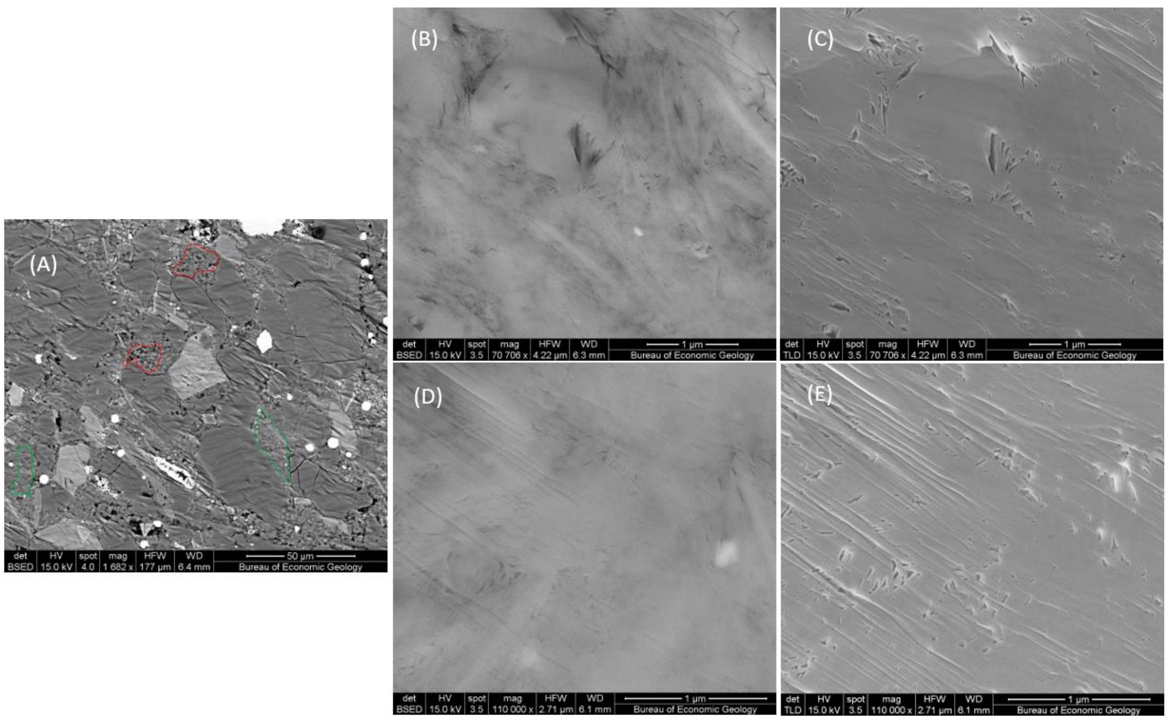

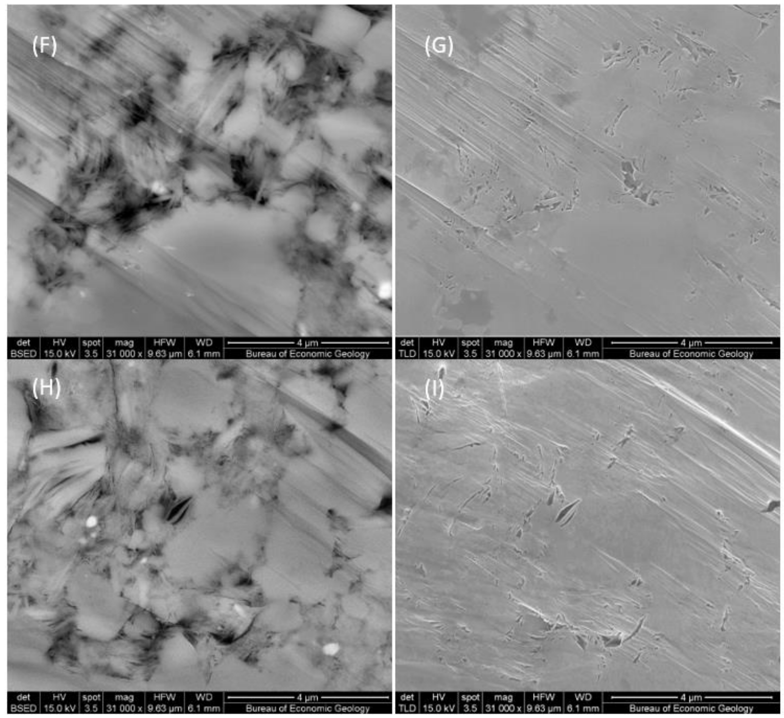

Fig. 6—SEM images of S1. (A) An overview showing the grayscale contrast in the porous areas between silt grains (10–50 μm); the green- and red-circled areas are the water-imbibed and residual oil areas, respectively; (B, D) example BSE images of typical areas in the two red-circled areas in (A); (C, E) the TLD images of (B) and (D); (F, H) example BSE images of typical areas in the two red-circled areas in (A); (G, I) the TLD images of (F) and (H).

The difference between the water-imbibed and residual oil areas lies in the pore size. Pores in the water-imbibed areas (**Figs. 6C**, **6E**) are generally smaller than those in the residual oil areas (**Figs. 6G**, **6I**). Note the larger scale bar in **Figs. 6G** and **6I** than that in **6C** and **6E**. Pores in the water-imbibed areas are no larger than 70 nm, whereas pores in the residual oil areas are up to approximately 300 nm.

Whereas clay mineral pores dominate in S1, small fractions of other types of pores also exist. The residual oil areas also contain small fractions of organic-matter pores (**Figs. A-2D**, **2E**) and intraparticle pores in pyrite framboids ("pyrite pores") (**Figs. A-2B**, **2C**) that contribute the very bright parts in **Fig. 3F**. The pyrite pores are either large in size or have an organic-matter boundary. Some dissolution-related intraparticle dolomite pores (not shown) are also included in the residual oil and water-imbibed areas.

Discussion on wettability and pore size effect. Two questions will be raised to initiate the discussion. First, are the residual oil areas (**Fig. 5A**) oil-wet? Second, why is there a major fraction of oil remaining in the residual oil areas if wettability is not the reason (**Fig. 5A**)?

It is clear that the water-imbibed areas are water-wet because water replaced oil and the major pore type is clay mineral pores. However, based on the results of water imbibition only, it can be erroneously interpreted that the residual oil areas are oil-wet. Oppositely, because the major pore type in the residual oil areas is also clay mineral pores according to the SEM analysis, these must be water-wet as well. The “aging” by the oil during oil imbibition and soaking have not changed the wettability in the water-imbibed areas and thus should not have changed the wettability in the residual-oil areas either. The organic-matter pores in the residual oil areas should be oil-wet, and the pyrite pores can be potentially oil-wet too; however, they only account for a small fraction of the pore volume and should not affect the overall wettability of the residual oil areas significantly. Because of the small fraction and the sparse distribution of the organic-matter and pyrite pores throughout the whole sample, it is reasonable to assume that they do not form an independently connected network; instead, they must be connected through the clay mineral pores in this sample.

Given the water-wet nature of the dominant clay mineral pores in the residual oil areas, the existence of the dominant oil in these pores can be attributed to the pore size effect on nonwetting phase capillary entrapment. It is well-documented that capillary entrapment of the nonwetting phase (oil herein) in the wetting phase (water) can occur more easily when the pore aspect ratio (pore body to throat ratio) is larger (Chatzis et al. 1983; Lenormand et al. 1983;

Tanino and Blunt 2012). When water enters a pore that is filled with oil, it will preferentially move around the corner of the pore first. When the water film approaches the narrow pore throat, a sudden merging of the water film (snap-off) will occur because of the interfacial force, then it continues to break through the pore throat and leaves the oil entrapped behind (Lenormand et al. 1983). The “snap-off” will occur when the pore throat is small and the pore body is significantly larger. By contrast, in pores that have a smaller pore aspect ratio, the snap-off may also occur, but with less oil left behind. This pore size effect was also observed in a previous study (Peng et al. 2019). In the residual oil areas, clay mineral pores have larger pore bodies, whereas they should have similar pore throat size to those in the water-imbibed areas, as indicated by the similar sizes of the smallest pores from the SEM images. Therefore, snap-off occurs more in the residual oil areas and a substantial fraction of oil is entrapped in the middle of the pore bodies, whereas the surface and pore throats of these pores are covered or filled with water. This process explains the answer to the second question raised above.

Note that if one relies on the SEM analysis of the dominant pore type only for S1, the correct conclusion to the water-wet nature of the pores can be reached as well. However, it may lead to overlooking the major fraction of residual oil in the sample. By contrast, if one relies on the imbibition test only, the erroneous conclusion can be drawn that half of the pores are oil-wet because approximately half of the oil remains. This example demonstrates the advantage of the integrated method used in this study: the comprehensive and more accurate understanding of water-oil displacement and the influencing factors, including wettability and pore size.

Sample 2 – a calcareous siliceous mudstone

Micro-CT image analysis. S2 shows a very different result for water-oil displacement from S1, with only a small fraction of oil recovery by water imbibition. Oil was imbibed in most porous areas in the dry sample between sand-sized calcite and quartz grains (~100–400 μm in size) (**Figs. 7A**, **7B**, and **7D**). After water imbibition, no obvious change can be seen in the central areas (**Fig. 7B** vs. **7C** and **Fig. 7D** vs. **7E**), and only slight changes on the edge of the sample (colored circled areas in **Fig. 7**), indicating little overall oil recovery by water imbibition, which is focused on the areas on the edge of the sample.

Interestingly, closer observation reveals that some oil redistribution after water imbibition occurred in this sample (**Fig. 8**, the red-boxed area in **Fig. 7A**). A few areas see the initially dark microscale pores become brighter (circled areas in **Fig. 8**). This result indicates that the pores were not filled with oil at the beginning, a reflection of the non-oil-wet nature of these pores, which then contained oil after water imbibition.

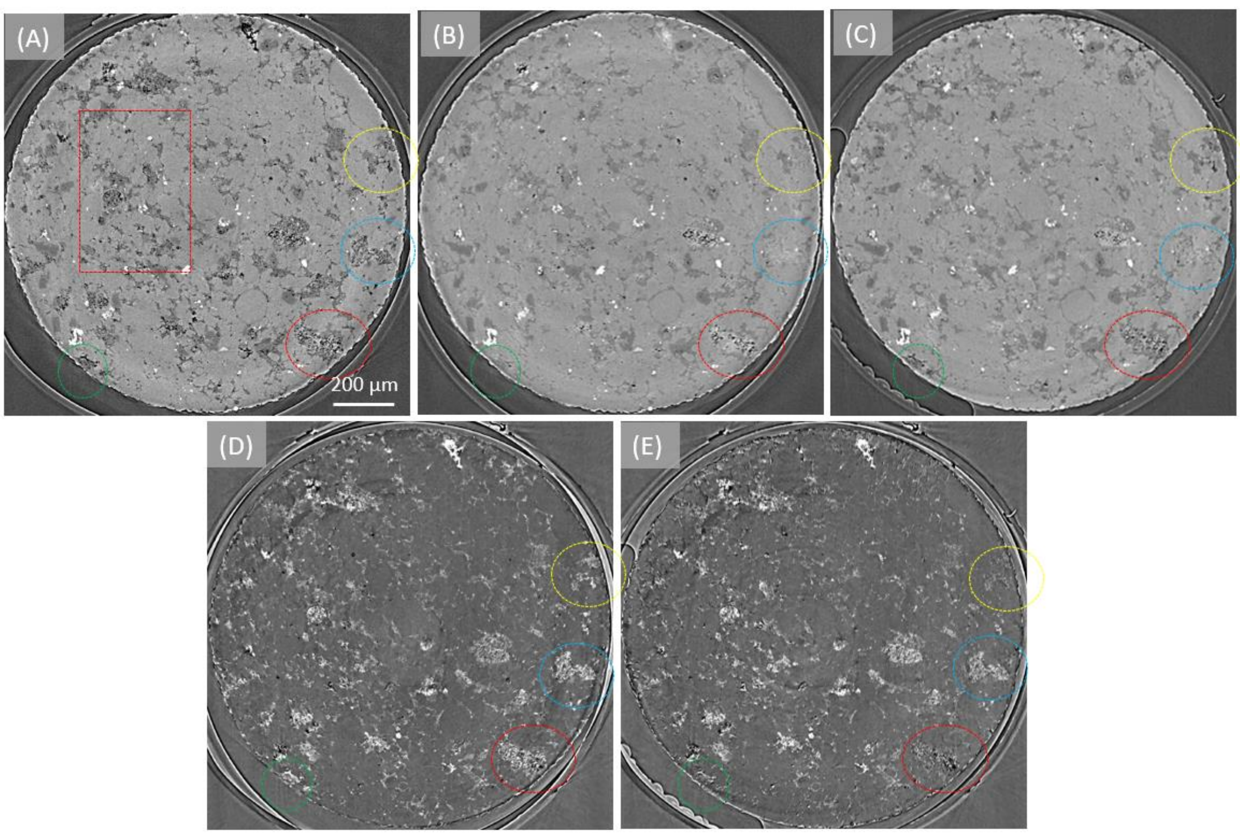

Fig. 7—Micro-CT images of S2 at different conditions and the image calculation results. (A) Dry sample; (B) after oil imbibition; (C) after water imbibition; (D) the difference image

between B and A (B – A); (E) the difference image between C and A (C – A). There is no obvious change after water imbibition, except in those areas in the circles.

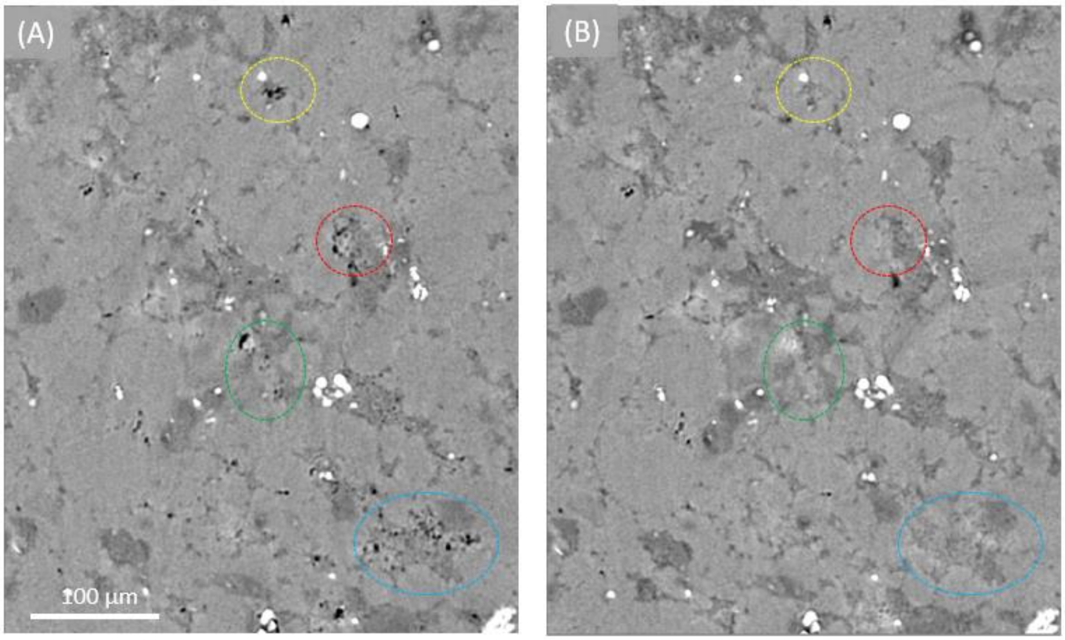

Fig. 8—Zoomed-in micro-CT images of the area in the red box in Fig. 7A. (A) After oil imbibition; (B) after water imbibition. The originally dark micropores in the circled areas after oil imbibition (A) become brighter after water imbibition (B), indicating oil redistribution in these areas.

Note that if there are some pores that are non-oil-wet, and later water imbibition into these pores (if any) does not contain oil, micro-CT imaging would not detect these pores. In that case, those water-wet pores can be overlooked. However, according to the imaging results, most porous areas between the grains are brighter in S2 (and the other two samples as well), indicating oil saturation in most porous areas in these samples. Therefore, the amount of such water-wet pores that may be overlooked are considered minimal in these samples.

SEM pore characterization. The dominant pore type in S2 is interparticle pores between microscale grains of calcite and quartz (**Fig. 9**). The porous areas with more calcite grains appear lighter than the area with more quartz grains (**Fig. 9B** vs. **9A**); however, no distinct oil recovery factor can be seen in either the darker or lighter areas in those areas on the edge of the sample (**Fig. 7**). For example, although the areas in the red-circled area are lighter than the yellow-circled area in **Fig. 7A**, the oil recovery by water imbibition in these two areas shows no distinct difference (**Fig. 7D** vs. **7E**).

Most pores in S2 have a mixed boundary of quartz and calcite (yellow-arrowed pores, **Fig. 9**). There are also some pores that have a quartz boundary only (green-arrowed pores, **Fig. 9**) or a calcite boundary (red-arrowed pores, **Fig. 9**). The pores in S2, which have a size up to a few microns (**Figs. 9B**, **9D**), are generally much larger than the clay mineral pores in S1. The EDS images show that a small fraction of clay mineral pores also exist in S2 (**Fig. A-3**). In addition, the sample also contains a very small fraction of organic-matter pores (images not shown).

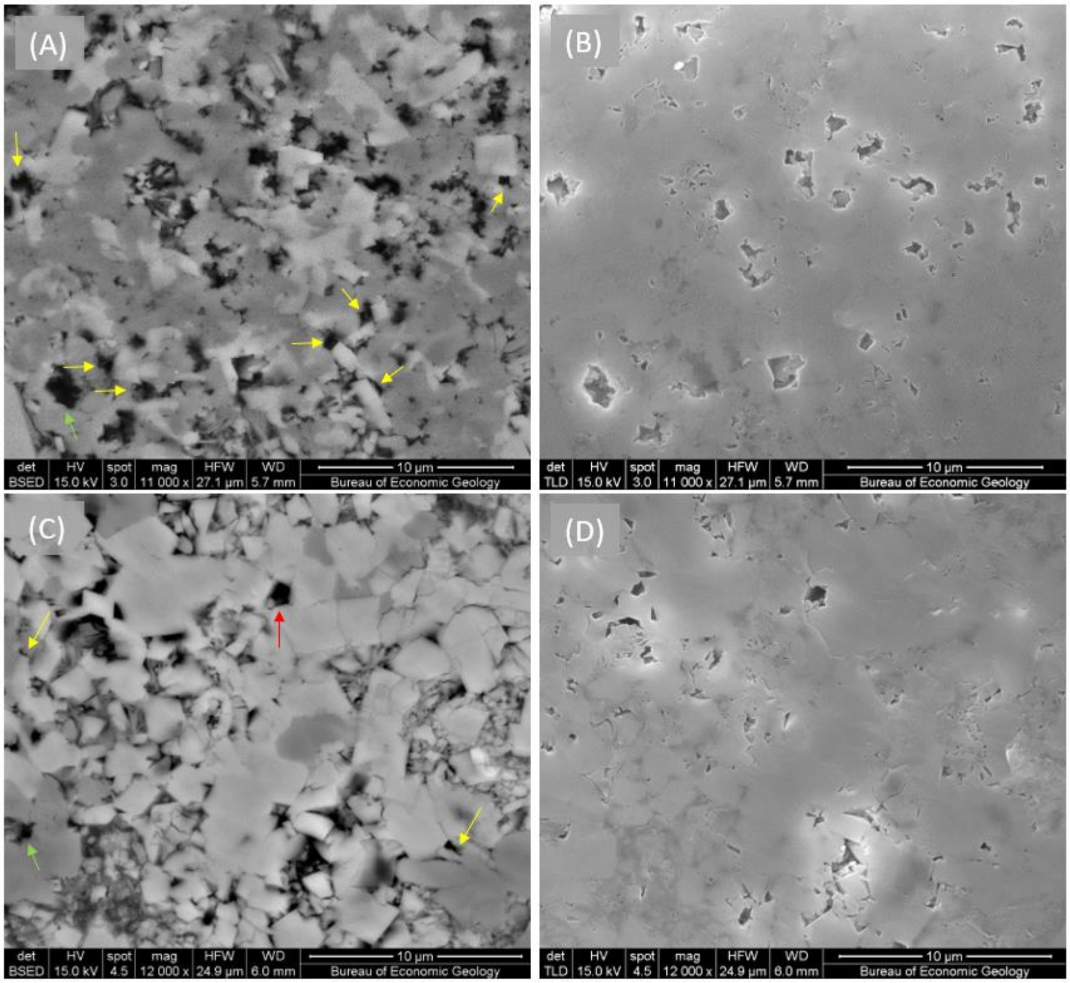

Fig. 9—SEM images of S2. (A, C) BSE images of two typical porous areas in S2; (C) has more calcite; yellow-arrowed pores have a mixed boundary of calcite and quartz; red-arrowed pores are calcite-bounded interparticle pores; green-arrowed pores are quartz-bounded interparticle pores. (B, D) the TLD images of (A, C), respectively.

Discussion on wettability and pore connection in S2. Three questions stand out for this sample. First, why was the overall oil recovery low and why did water-oil displacement only occur on the edge? Second, what is the cause of the oil redistribution? Third, what do the observations from micro-CT and SEM images reveal about the sample with respect to wettability and other controlling factors?

To find the answers to these questions, we use the process of elimination for several presuppositions. 1) Pores in S2 are oil-wet. Although this assumption can explain why there was no oil recovery by water imbibition in most areas in the middle of the sample, it cannot explain why oil recovery has occurred in the porous areas on the edge where the pore types are no different from those in the middle. 2) Pores in S2 are water-wet, but the connectivity of water-wet pores in the middle is poor. Similar pore connectivity analysis of the residual oil and water-imbibed areas as that for S1 was conducted for the porous areas in the red-circled area in **Fig. 7**. It can be seen that both residual oil and water-imbibed areas have good connectivity (**Fig. A-4**). The overall pore connection in the middle of the sample is good as well (**Fig. A-4C**). Again, there is no distinct difference in the pore type between the areas in the middle and in the edge; therefore, pore connection of different pore types should also be similar in these two areas. Thus, if most pores in S2 were water-wet and we now understand that pore connectivity is not a hurdle, then evident oil recovery would have occurred in the middle of the sample.

Therefore, the analysis above indicates that the sample is neither oil-wet nor water-wet and that pore connection is not a limiting factor for limited oil recovery. The only explanation is that the pores are mostly intermediate-wet or neutral. This can be related to the fact that the majority of the pores consist of mixed calcite and quartz boundaries, and the calcite tends to be more oil-wet and the quartz more water-wet. The combination of this mixed wettability in an individual pore makes the pore have a neutral- or close-to-neutral wetting nature, and the imbibition of water in the oil-presaturated sample is thus very slow and only occurs on the edge of the sample/water interface through the process of countercurrent diffusion.

Note that wettability is relative to a specific fluid pair. Oil imbibition in the dry sample indicates that most pores are oil-wet relative to air. Nevertheless, pores in S2 are not all oil-wet relative to air, as indicated by the oil redistribution, that is, pores without oil originally contain oil after water imbibition. These pores must be the quartz-bounded pores. They do not appear to be oil-wet in S2, even relative to air. Instead, they are more water-wet, and because of the large size of these pores (microscale pores), oil entered the water-wet pores by cocurrent flow with water as entrapped, phase driven by the capillary force of the quartz pores. This observation-based speculation explains the reason for the oil redistribution in some pores.

Therefore, S2 is mostly intermediate-wet with a small fraction of pores being more water-wet. It is reasonable to assume that the other small fraction of calcite-only pores is more oil-wet. The overall pore connection is good and is not a limiting factor for water-oil displacement. The more water-wet pores are more likely to be connected through the intermediate-wet pore network instead of having an independent pore network. This is in accord with the observation that there is no obvious oil recovery overall and yet some oil-redistribution in the middle. Because of the very small amount of organic matter pores in S2, no independently connected organic matter pore network shall exist.

It is important to differentiate intermediate-wet from mixed-wet. S2 is intermediate-wet, not mixed-wet. Intermediate-wet, as shown by the water imbibition result in S2, is a neutral wetting nature that makes the pores favor neither water or oil spontaneous imbibition. Mixed-wet, instead, is that a part of the pores in a sample is water-wet, and the other is oil-wet; therefore, water imbibition in a part of the sample would be observed if S2 were mixed-wet.

Sample 3 – an organic-matter-rich calcareous mudstone

S3 is a relatively simple sample compared to the previous two. Essentially no water-oil displacement has occurred in S3 based on the micro-CT images (**Fig. 10**). This sample has smaller grains (<2–4 μm) than S1 and S2, and thus the porous areas appear to be distributed across the whole sample as indicated by the result of oil imbibition (**Fig. 10D**). The brightness of the oil-imbibed areas does not show any sign of change after water imbibition, indicating no (or minimal) occurrence of water-oil displacement.

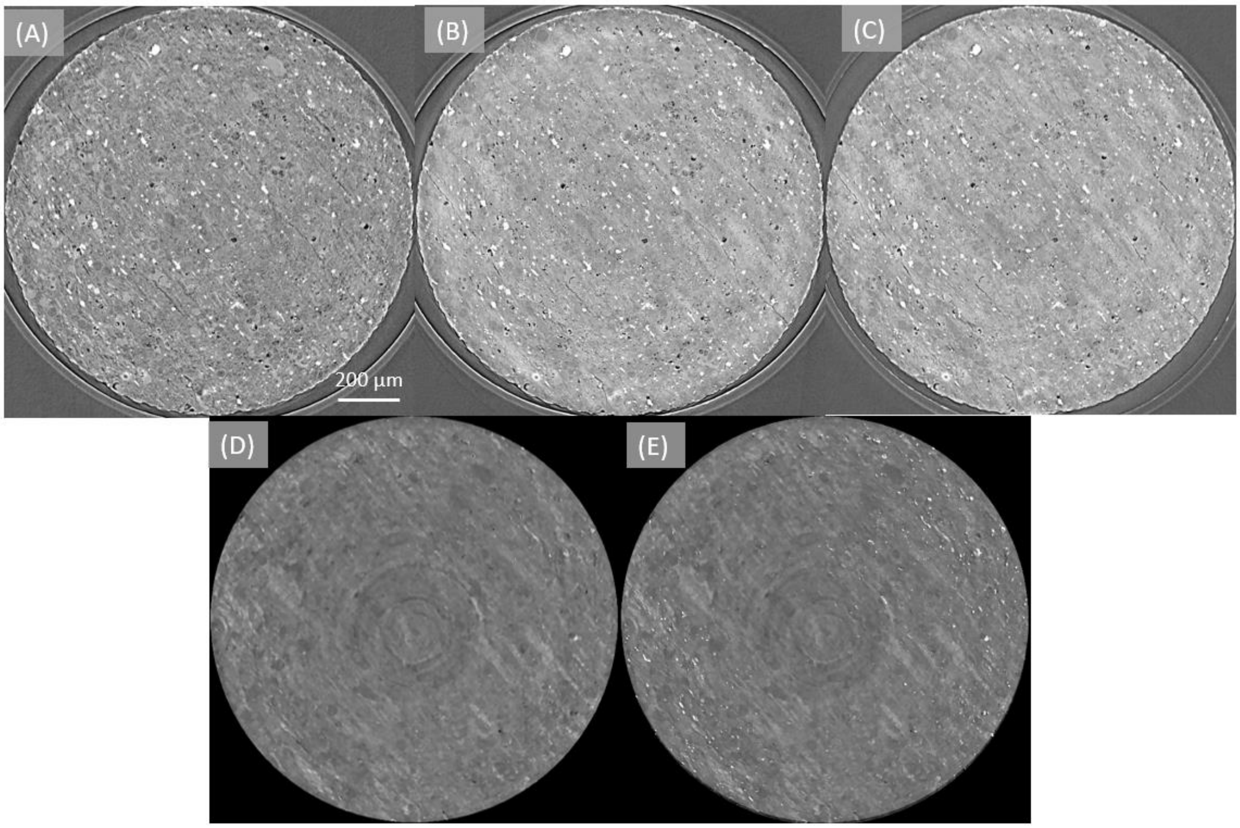

Fig. 10—Micro-CT images of S3 at different conditions and the image calculation results. (A) Dry sample; (B) after oil imbibition; (C) after water imbibition; (D) the difference image between B and A (B – A); (E) the difference image between C and A (C – A). There is no sign of change after water imbibition in any of the porous areas in this sample. The small, very bright spots are the result of very small errors in image registration and are artifacts.

Sample S3 is therefore considered more oil-wet. This is confirmed by the SEM pore characterization. There are two types of dominant pores in S3: calcite pores and organic-matter pores, both of which are more oil-wet. The former are calcite pores in coccoliths and are much larger (up to 1–2 µm) than the latter (**Fig. 11**). A part of the calcite pores has at least some boundary of organic matter, interpreted to be migrated bitumen (**Figs. 11B**, **11D**). The pores within the organic matter are smaller (<300 nm) but very common (**Fig. 11D**). A substantial amount of spongy organic-matter pores of even smaller size (<20 nm) exists in the organic matter inside the foraminifer chambers (**Fig. A-5**). Note that S3 demonstrates layered distributed pore networks (**Fig. 10D**), some having brighter grayscale than others. The brighter layer indicates larger pores and is thus interpreted to consist of the larger calcite pores, whereas the other layers include the smaller organic pores. In other words, the calcite and organic-matter pores may form independently connected pore networks in this sample.

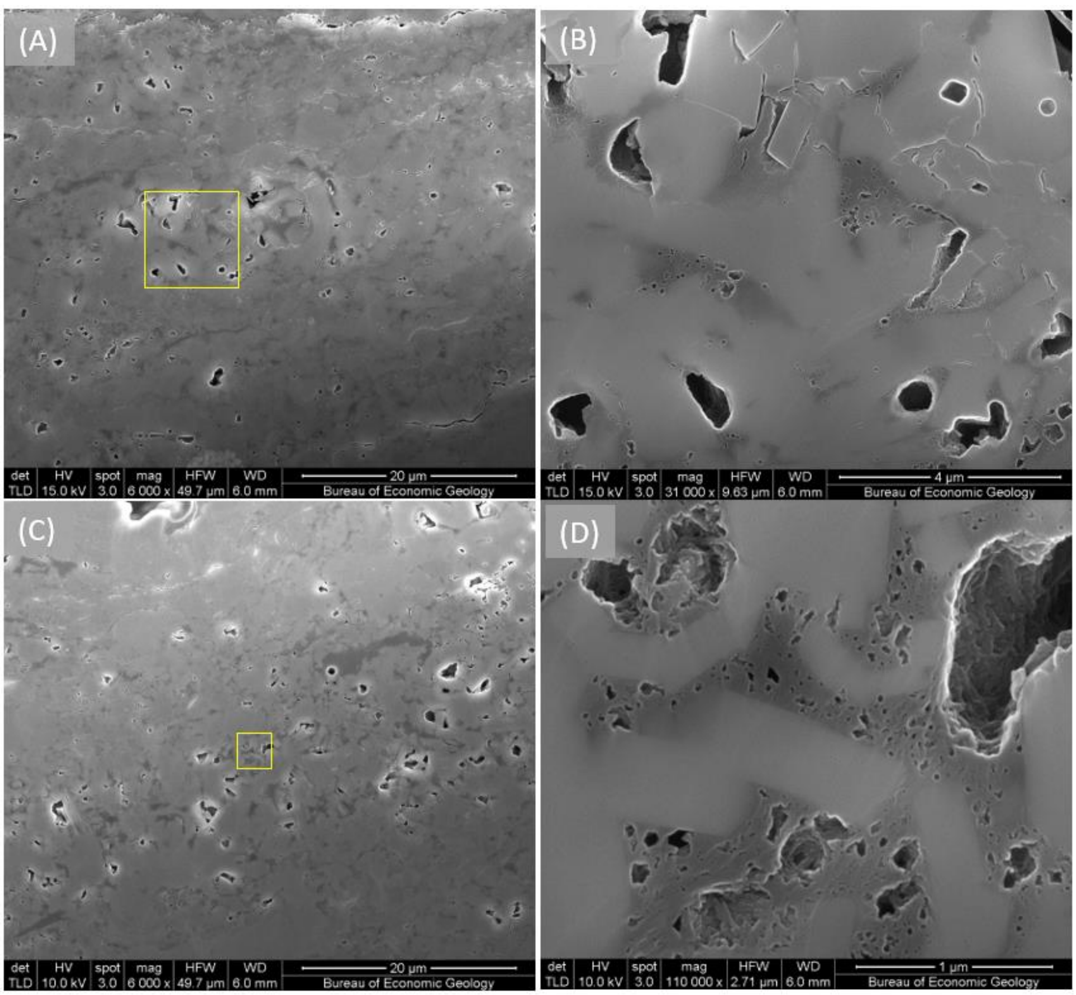

Fig. 11—SEM images of S3. (A, C) Example TLD images showing the distribution of the large calcite pores and the organic matter; (B, D) the magnified area of the yellow box in (A, C),

respectively, showing the coexistence of the larger calcite pores and the smaller organic-matter pores. A large number of the calcite pores have clean calcite boundaries in (B); (D) shows the big calcite pores with an organic-matter (most likely migrated bitumen) boundary.

Implications on improved oil recovery strategies

Although the experiment in this study was conducted under ambient conditions, to a certain extent the results of water-oil distribution after water imbibition can reflect the subsurface situation after hydraulic fracturing with respect to water-oil distribution in the shale matrix. The results therefore have important implications on water cut source analysis, fracturing fluid selection, and potential improved oil recovery strategies. The discussion below is based on the assumption that each sample (S1–S3) represents a major type of lithofacies of the reservoir.

S1. Because of its water-wet nature, water enters most of the pores (clay mineral pores) in this sample. In subsurface conditions, the smaller clay mineral pores, such as those pores smaller than 70 nm, may have been occupied by water even before hydraulic fracturing. In the relatively larger pores (>70 nm), oil exists but is entrapped in the middle of the pore bodies by water after hydraulic fracturing. This water-oil distribution favors water flow but hinders oil flow. Therefore, the water relative permeability is high, whereas the oil relative permeability is low even though the oil saturation is still high (for example, ~50% after water imbibition in this experiment). This phenomenon can partly explain the causes of high water cut from this type of reservoir in Wolfcamp plays.

To reduce the water-block effect, less water-wetting fracturing fluid should be applied, if possible. A fracturing fluid containing a surfactant-type additive that can enhance the solubility of oil in water and reduce the surface tension between water and oil would also be beneficial.

Because of the strong water blocking effect in this sample, gas injection, such as "huff and puff," would not be efficient. Gas relative permeability will be low in this type of reservoir, and the accessibility of gas to the entrapped oil is limited at the same time. Therefore, improving the oil solubility and/or reducing the water blocking effect should be the preferred strategy for this type of reservoir.

S2. Water imbibition into the well-connected pore system in S2 is slow because of the intermediate-wetting property of the majority of pores. Therefore, slight water uptake to a minimal depth near the fracture-matrix interface can be expected after hydraulic fracturing, and the water-block effect should be minor, which is beneficial to post-fracturing oil flow.

To further enhance the production after primary depletion in this type of reservoir, both wettability alteration and miscible gas injection may work. Considering that the quartz part of the pore boundary is water-wet, wettability alteration should be focused mainly on the calcite part. However, because the water-block effect may occur after initial improved oil production due to water imbibition, the long-term production can be restrained. In this sense, miscible gas injection may be a better option prior to wettability alteration. Good pore connectivity in this sample warrants the flow path of either a water-based wettability alterating agent or gas.

S3. For an organic-matter-rich calcareous mudstone in which calcite and organic-matter pores are dominant, water imbibition after hydraulic fracturing should be minimal. Even if there is certain initial water saturation before hydraulic fracturing, the oil should still be distributed in organic matter pores that are oil-wet. Therefore, miscible gas injection may be a good option for this type of reservoir. Wettability alteration can be difficult for the organic-matter pores; however, it may work for the calcite pores. Because the calcite pores and organic-matter pores are very likely to have independent pore networks, the water block effect due to water imbibition will not affect the oil-wet organic-matter pore network; therefore, the methods of wettability alteration targeted for the calcite pores and miscible gas injection for the organic-matter pores may be applied at the same time without interfering with each other.

In reality, different lithologies of rocks always exist in a reservoir; thus, comprehensive consideration based on the accurate understanding of each type of rock and its weight in the reservoir must be taken into account for the optimal improved oil recovery strategy. Also note that the suggested EOR strategies in this paper are based on the analysis of wettability and water-oil displacement, more practical factors such as fracture connectivity and communication, possible early gas breakthrough and instable gas-fluid interface in gas injection, existing infrastructure and cost should be taken into account in the actual decision-making.

Conclusions

This comparative study of three samples with different types of pore systems, lithologies, and wettability provided an improved understanding of the mechanisms of water-oil displacement by imbibition and its controlling factors, including wettability, pore size (aspect ratio), and pore connectivity. While shale is commonly considered to be mixed-wet, it is important to have an accurate understanding of how mixed the wettability is, what its distribution is, and how it affects oil distribution. Wettability is easier to evaluate for pores with a certain type of mineral or organic-matter boundary; however, it is not straightforward for pores with boundaries of different types of minerals (such as intermediate-wet in S2). Wettability is a key factor in determining water-oil displacement. Comparison of the three samples shows that S1, which is more water-wet, has the higher oil recovery than S2 and S3, which are intermediate-wet and oil-wet, respectively. Nevertheless, wettability is not the only influencing factor for water-oil displacement. For samples that are similar to S1, pore size, specifically pore aspect ratio, also plays an important role. Wettability is a surface property, and should not be equalized with oil recovery or oil/water dominance in a sample, which are volume-based parameters. Independent pore networks with different wettability may not exist in a specific sample as previously assumed by many researchers. The connectivity of the pores with specific wettability is dependent on the fraction of the specific pores. The dominant type of pore in a sample is generally well-connected, whereas non-dominant pores do not have an independently connected network. Instead, they are commonly connected with the dominant pore network.

Application of this integrated imaging and imbibition method for shale samples in major lithofacies will be necessary for a full comprehension of pore wettability, water-oil displacement, and water-oil distribution in a specific formation. Specific strategy of improved oil recovery can be obtained for specific rock types based on the integrated analysis. This integrated technique also provides a promising way for further studies of the influence of fluid composition, such as brine salinity, pH, and oil components, on pore wettability and water-oil displacement.

Acknowledgments

This study is sponsored by The University of Texas at Austin Startup Fund for Sheng Peng, Project STARR (State of Texas Advanced Oil and Gas Resource Recovery), and the Mudrock Systems Research Laboratory (MSRL) of the Bureau of Economic Geology at UT Austin. We thank MSRL sponsors (http://www.beg.utexas.edu/msrl/sponsors) for their support. William Rader edited the paper. Publication authorized by the Director, Bureau of Economic Geology.

References

Ali, M., Ali, S., Mathur, A. and Belanger, C. 2020. Organic Shale Spontaneous Imbibition and Monitoring with NMR to Evaluate In-Situ Saturations, Wettability and Molecular Sieving. Unconventional Resources Technology Conference (URTeC), Virtual, 20–22 July. doi: 10.15530/urtec-2020-3096.

Alvarez, J. and Schechter, D.S. 2017. Wettability alteration and spontaneous imbibition in unconventional liquid reservoirs by surfactant additives. Society of Petroleum Engineers Reservoir Evaluation and Engineering SPE-177057-PA.

Arif, M., Zhang, Y. and Iglauer, S. 2021. Shale Wettability: Data Sets, Challenges, and Outlook. *Energy Fuels* **35** (4): 2965–2980.

Begum, M., Yassin, M.R. and Dehghanpour, H. 2019. Effect of kerogen maturity on organic shale wettability: A Duvernay case study. *Mar. Pet. Geol.* **110**: 483– 496.

Borysenko, A., Clennell, B., Sedev, R., Burgar, I., Ralston, J., Raven, M., Dewhurst, D. and Liu, K. 2009. Experimental investigations of the wettability of clays and shales. *J Geophys Res Solid Earth* **114**: 1–11.

Chatzis, I., Morrow, N.R. and Lim, H.T. 1983. Magnitude and detailed structure of residual oil saturation. Society Petroleum Engineers Journal **23** (2): 311–326.

Chen, Y., Xie, Q., Sari, A., Brady, P.V. and Saeedi, V. 2018. Oil/Water/Rock Wettability: Influencing Factors and Implications for Low Salinity Water Flooding in Carbonate Reservoirs. *Fuel* **215**: 171-177.

Dick, M.J., Veselinovic, D., Green, D., Scheffer-Villarreal, A., Bonnie, R.J.M., Kelly, S. and Bower, K. 2019. "NMR Wettability Index Measurements on Unconventional Samples." Unconventional Resources Technology Conference, Denver, CO, USA, 22–24 July.

Engelder, T., Cathles, L.M. and Bryndzia, L.T. 2014. The fate of residual treatment water in gas shale. *Journal of Unconventional Oil and Gas Resources* **7**: 33–48.

Fletcher, P. and Nicholls, R.J. 2000. Alkylbenzenes in Diiodomethane. A Novel, "Primitive" Micelle-Forming Surfactant System. *Langmuir* **16**: 1050–1056.

Fogden, A., Latham, S., McKay, T., Marathe, R., Turner, M., Kingston, A. and Senden, T. 2014a. Micro-CT analysis of pores and organics in unconventionals using novel contrast strategies. Unconventional Resources Technology Conference, Denver, Colorado, USA, 25–27 August.

Fogden, A., Middleton, J., McKay, T., Latham, S., Marathe, R., Turner, M., Sheppard, A., Howard, C.J.J. and Lane, F.D. 2014b. 3D mapping of pore and organic matter distributions in unconventional reservoirs utilizing a digital rocks approach. International Symposium of the Society of Core Analysts, Avignon, France, 8–11 Sept.

Gao, Z. and Hu, Q. 2016. Wettability of Mississippian Barnett Shale samples at different depths: Investigations from directional spontaneous imbibition. *Am Assoc Pet Geol Bull* **100**: 101–114.

Gao, Z., Fana, Y., Hu, Q., Jiang, Z., Cheng, Y. and Xuan, Q. 2019. A review of shale wettability characterization using spontaneous imbibition experiments. *Marine and Petroleum Geology* **109**: 330–338

Gupta, I., Jernigen, J., Curtis, M., Rai, C. and Sondergeld, C. 2018.Water-Wet or Oil-Wet: Is It Really That Simple in Shales? *Petrophysics* **59**, (3): 308–317.

Jagadisan, A. and Heidari, Z. 2019. Experimental Quantification of the Effect of Thermal Maturity of Kerogen on Its Wettability. *SPE Reservoir Eval. Eng.* **22** (04): 1323–1333.

Kelly, S.R.J., Bonniel, R.J.M., Dick, M.J. and Veselinovic, D. 2020. NMR Time-Lapse Wettability Assessments in Unconventionals: Insights from Imbibition. Unconventional Resources Technology Conference, Virtual, 20–22 July.

Ketcham, R.A. and Carlson, W.D. 2001. Acquisition, optimization and interpretation of X-ray computed tomographic imagery: Applications to the geosciences. *Computers & Geosciences* **27** (4): 381–400.

Ko, L.T., Loucks, R.G., Ruppel, S.C., Zhang, T. and Peng, S. 2017. Origin and characterization of Eagle Ford pore networks in the south Texas Upper Cretaceous shelf. *AAPG Bull.* **101** (3): 387–418.

Lan, Q., Xu, M., Binazadeh, M., Dehghanpour, H. and Wood, J.M. 2015. A comparative investigation of shale wettability: the significance of pore connectivity. *J. Nat. Gas Sci. Eng.* **27**: 1174–1188.

Lenormand, R., Zarcone, C. and Sari, A. 1983. Mechanisms of the displacement of one fluid by another in a network of capillary ducts. *J Fluid Mech* **135**: 337–353.

Looyestijn, W.J. and Hofman, J. 2006. Wettability-Index Determination by Nuclear Magnetic Resonance. *SPE Res Eval & Eng* **9** (02): 146–153.

Lu, Y., Zeng, L., Sari, A., Chen, Y., Jin, Y. and Xie, Q. 2019. Wetting Behavior of Shale Rocks and Its Relationship to Oil Composition. *Energy Fuels* **33** (12): 12270–12277.

Makhanov, K., Dehghanpour, H. and Kuru, E. 2012. An experimental study of spontaneous imbibition in Horn River shales. In SPE Canadian Unconventional Resources Conference, Calgary, Alberta, Canada, October 30–November 1. SPE 162650.

Pan, B., Li, Y., Zhang, M., Wang, X., Iglauer, S. 2020a. Effect of total organic carbon (TOC) content on shale wettability at high pressure and high temperature conditions. *Journal of Petroleum Science and Engineering*, 193, https://doi.org/10.1016/j.petrol.2020.107374

Pan, B., Yin, X. and Iglauer, S. 2020b. A review on clay wettability: From experimental investigations to molecular dynamics simulations. *Adv. Colloid Interface Sci.* **285:** 102266. doi: 10.1016/j.cis.2020.102266

Peng, S. and Xiao, X. 2017. Investigation of multiphase fluid imbibition in shale through synchrotron-based dynamic micro-CT imaging. *J Geophys Res Solid Earth* **122**: 4475–4491.

Peng, S., Liu, Y., Ko, L. and Ambrose, W. 2019a. Water/Oil Displacement by Spontaneous Imbibition Through Multiscale Imaging and Implication on Wettability in Wolfcamp Shale. Unconventional Resources Technology Conference, July 22–24, Denver, Colorado. doi:10.15530/urtec-2019-194.

Peng, S., Ren, B. and Meng, M. 2019b. Quantifying the influence of fractures for more accurate laboratory measurement of shale matrix permeability using a modified gas expansion method. SPE-195570-PA. doi:10.2118/195570-PA.

Roshan, H., Andersen, M.S., Rutlidge, H., Marjo, C.E. and Acworth, R.I. 2016. Investigation of the kinetics of water uptake into partially saturated shales. *Water Resour Res* **52**: 2420–2438.

Schembre, J., Akin, S. and Kovscek, A.R., 1998. Spontaneous Imbibition in Low Permeability Media. PhD dissertation, Stanford University, Stanford, California 94305, USA.

Schneider, C., Rasband, W.S. and Eliceiri, K.W. 2012. NIH Image to ImageJ: 25 years of image analysis. *Nat Methods* **9**: 671–675.

Siddiqui, M.A.Q., Ali, S., Fei, H. and Roshan, H. 2018. Current understanding of shale wettability: A review on contact angle measurements. *Earth-Science Reviews* **181**: 1–11.

Singh, H. 2016. A critical review of water uptake by shales. *J Nat Gas Sci Eng* **34**: 751–766.

Tanino, Y. and Blunt, M.J. 2012. Capillary trapping in sandstones and carbonates: Dependence on pore structure. *Water Resour Res* **48**: W08525. doi: 10.1029/2011WR011712.

Yassin, M.R., Dehghanpour, H., Wood, J. and Lan, Q. 2016. A theory for relative permeability of unconventional rocks with dual-wettability pore network. *Society Petroleum Engineers Journal* SPE-178549-PA.

Yassin, M.R., Begum, M. and Dehghanpour, H. 2017. Organic shale wettability and its relationship to other petrophysical properties: a Duvernay case study. *Int. J. Coal Geol.* **169**: 74–91.

Appendix

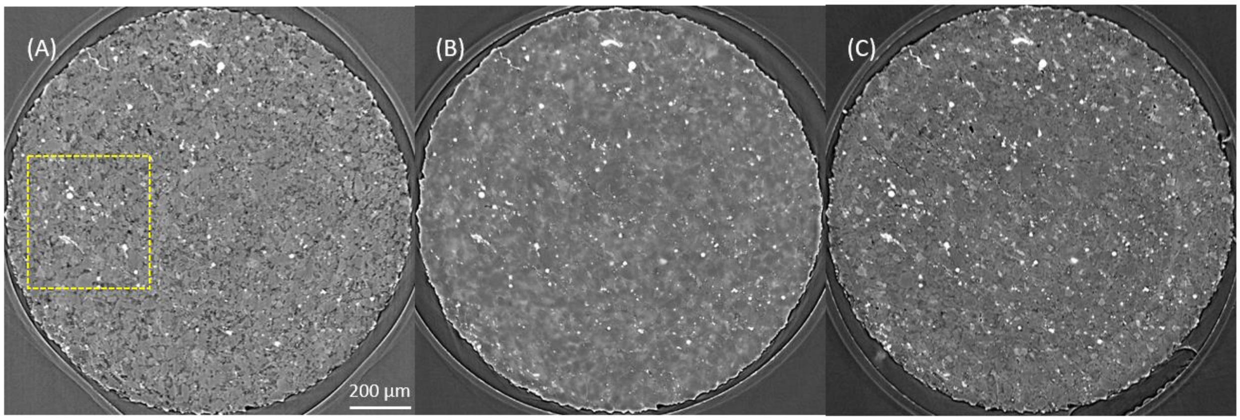

Fig. A-1—Registered micro-CT images of S1. (A) dry; (B) after oil imbibition; (C) after water imbibition. The diameter of the sample is 1.5 mm. The area in the yellow box is zoomed in and shown in Fig. 2 in the main text.

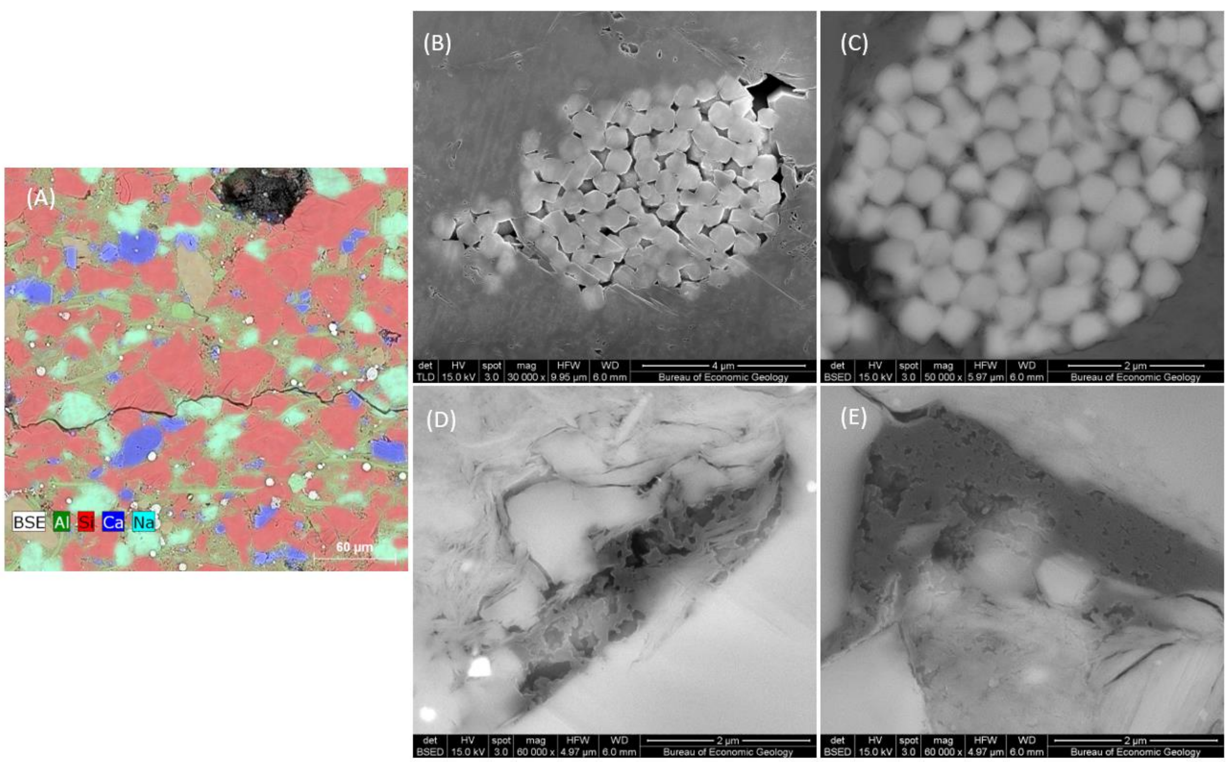

Fig. A-2—EDS and SEM images for S1. (A) EDS map showing clay minerals (green) as the dominant minerals in the porous areas; (B, C) two examples of interparticle pores in pyrite framboids that have either a big size or an organic-matter boundary; (D, E) two examples of organic-matter pores.

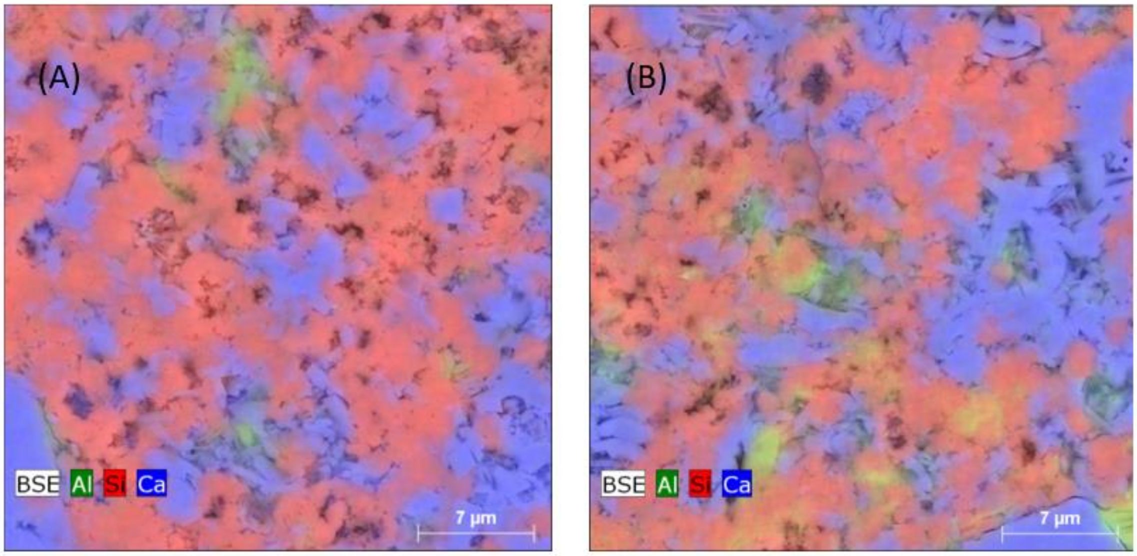

Fig. A-3—EDS maps for S2. The porous areas consist of microscale quartz (red) and calcite (blue) grains. A major part of the interparticle pores has a mixed boundary of quartz and calcite.

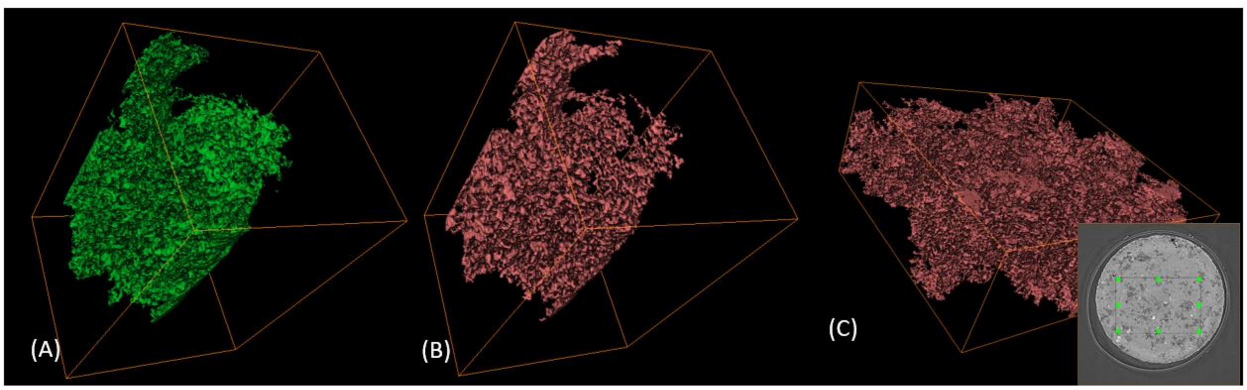

Fig. A-4—(A) 3D image of the water-imbibed areas in a local area (red-circled area in Fig. 7) on the edge in S2; (B) 3D image of the residual oil areas in the same area; (C) overall porous areas in S2 in the green-boxed area of the sample. These images show good connectivity of all these areas.

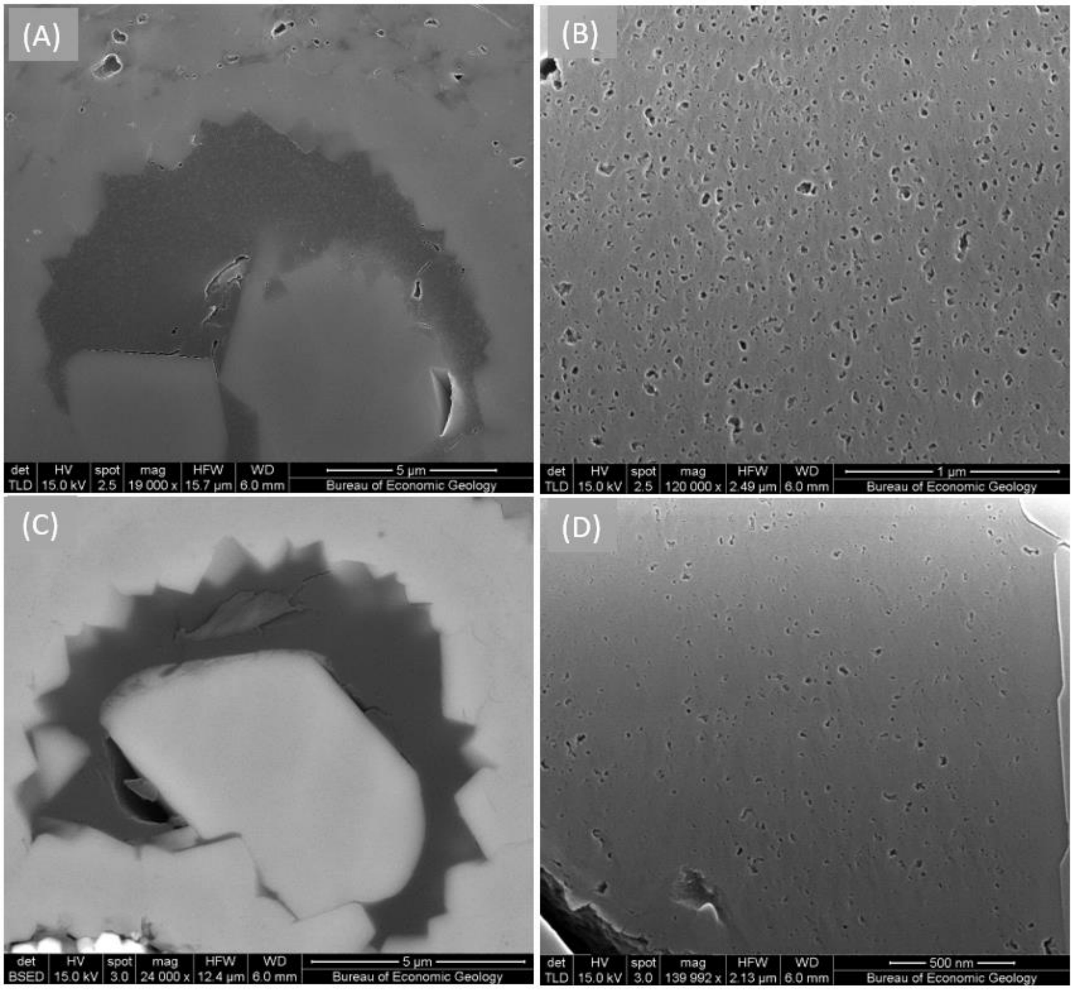

Fig. A-5—Example SEM images of the small (<20 nm), spongy organic-matter pores in S3. (A, C) BSE images showing the organic matter with pores in foraminifer chambers. (B, D) TLD images showing the spongy pores (<20 nm) in the organic matter in (A, C), respectively.

Figure Captions

Fig. 1—Contact angle measurement of DIM, DIM+C12B, and the paraffin oil on a glass plate. (A) Snapshots of the sessile drop tests; (B) comparison of the contact angle.

Fig. 2—Micro-CT images of S1 at different conditions and the image calculation/processing results. (A) Dry scan; (B) after oil imbibition; (C) result image of (B – A), lighter areas are where oil imbibition occurs; (D) segmentation result of C, yellow represents oil-imbibed areas; (E) after water imbibition; (F) result image of (E – A), lighter areas contain residual oil after water-oil displacement; (G) segmentation result of F, red represents residual oil areas.

Fig. 3—Image calculation/processing results of the images shown for S1 in Fig. 2. (A) The combination of water-imbibed areas (green) and residual oil areas (red) with the dry image in background; (B) water-imbibed areas (green); (C) residual oil areas (red); (E) extracted areas of green in (B) from the dry image, showing the areas with water imbibition in the dry sample; (F) extracted areas of red in (C) from the dry image, showing the areas with residual oil in the dry sample.

Fig. 4—Residual oil factor map (B) in water-imbibed and residual oil areas (A). Red and green in (A) denote the residual oil and water-imbibed areas, respectively. Scale bar in (B) is the residual oil factor after water imbibition from 0 to 1.0.

Fig. 5—3D images showing the independently connected networks of the residual oil areas (A) and the water-imbibed areas (B). These two networks are interconnected at the same time in the 3D space (C).

Fig. 6—SEM images of S1. (A) An overview showing the grayscale contrast in the porous areas between silt grains (10–50 µm); the green- and red-circled areas are the water-imbibed and residual oil areas, respectively; (B, D) example BSE images of typical areas in the two red-circled areas in (A); (C, E) the TLD images of (B) and (D); (F, H) example BSE images of typical areas in the two red-circled areas in (A); (G, I) the TLD images of (F) and (H).

Fig. 7—Micro-CT images of S2 at different conditions and the image calculation results. (A) Dry sample; (B) after oil imbibition; (C) after water imbibition; (D) the difference image between B and A (B – A); (E) the difference image between C and A (C – A). There is no obvious change after water imbibition, except in those areas in the circles.

Fig. 8—Zoomed-in micro-CT images of the area in the red box in Fig. 7A. (A) After oil imbibition; (B) after water imbibition. The originally dark micropores in the circled areas after oil imbibition (A) become brighter after water imbibition (B), indicating oil redistribution in these areas.

Fig. 9—SEM images of S2. (A, C) BSE images of two typical porous areas in S2; (C) has more calcite; yellow-arrowed pores have a mixed boundary of calcite and quartz; red-arrowed pores are calcite-bounded interparticle pores; green-arrowed pores are quartz-bounded interparticle pores. (B, D) the TLD images of (A, C), respectively.

Fig. 10—Micro-CT images of S3 at different conditions and the image calculation results. (A) Dry sample; (B) after oil imbibition; (C) after water imbibition; (D) the difference image between B and A (B – A); (E) the difference image between C and A (C – A). There is no sign of

change after water imbibition in any of the porous areas in this sample. The small, very bright spots are the result of very small errors in image registration and are artifacts.

Fig. 11—SEM images of S3. (A, C) Example TLD images showing the distribution of the large calcite pores and the organic matter; (B, D) the magnified area of the yellow box in (A, C), respectively, showing the coexistence of the larger calcite pores and the smaller organic-matter pores. A large number of the calcite pores have clean calcite boundaries in (B); (D) shows the big calcite pores with an organic-matter (most likely migrated bitumen) boundary.

Fig. A-1—Registered micro-CT images of S1. (A) dry; (B) after oil imbibition; (C) after water imbibition. The diameter of the sample is 1.5 mm. The area in the yellow box is zoomed in and shown in Fig. 2 in the main text.

Fig. A-2—EDS and SEM images for S1. (A) EDS map showing clay minerals (green) as the dominant minerals in the porous areas; (B, C) two examples of interparticle pores in pyrite framboids that have either a big size or an organic-matter boundary; (D, E) two examples of organic-matter pores.

Fig. A-3—EDS maps for S2. The porous areas consist of microscale quartz (red) and calcite (blue) grains. A major part of the interparticle pores has a mixed boundary of quartz and calcite.

Fig. A-4—(A) 3D image of the water-imbibed areas in a local area (red-circled area in Fig. 7) on the edge in S2; (B) 3D image of the residual oil areas in the same area; (C) overall porous areas in S2 in the green-boxed area of the sample. These images show good connectivity of all these areas.

Fig. A-5—Example SEM images of the small (<20 nm), spongy organic-matter pores in S3. (A, C) BSE images showing the organic matter with pores in foraminifer chambers. (B, D) TLD images showing the spongy pores (<20 nm) in the organic matter in (A, C), respectively.